

# Towards General Purpose and Geometry Preserving Single-View Depth Estimation

\*Mikhail Romanov  
 Samsung AI Center Moscow  
 m.romanov@samsung.com

\*Nikolay Patakin  
 Samsung AI Center Moscow,  
 Higher School of Economics  
 n.patakin@samsung.com

Anna Vorontsova  
 Samsung AI Center Moscow,  
 Higher School of Economics  
 a.vorontsova@samsung.com

Anton Konushin  
 Samsung AI Center Moscow,  
 Moscow State University  
 a.konushin@samsung.com

July 2020

## Abstract

Single-view depth estimation plays a crucial role in scene understanding for AR applications and 3D modelling as it allows to retrieve the geometry of a scene. However, it is only possible if the inverse depth estimates are unbiased, *i.e.* they are either absolute or Up-to-Scale (UTS). In recent years, great progress has been made in general-purpose single-view depth estimation. Nevertheless, the latest general-purpose models were trained using ranking or on Up-to-Shift-Scale (UTSS) data. As a result, they provide UTSS predictions that cannot be used to reconstruct scene geometry. In this work, we strive to build a general-purpose single-view UTS depth estimation model. Following Ranftl *et al.*, we train our model on a mixture of datasets and test it on several previously unseen datasets. We show that our method outperforms previous state-of-the-art UTS models. We train several light-weight models following the proposed training scheme and prove that our ideas are applicable for computationally efficient depth estimation.

## 1 Introduction

Single-view monocular depth estimation is essential for understanding geometry of a 3D scene and has been studied for decades. Classical depth estimation methods use various efficient and inventive ways of utilizing image data, and seek helpful cues in visual data through detecting edges, estimating planes, or matching objects. Recently, deep learning-based approaches started to compete with classical computer vision algorithms that make use of hand-crafted features. The major advances in this area imply training convolutional neural networks to estimate the real-valued depth map from RGB image.

Diverse training data is necessary for training a model able to perform in various real-world scenarios.

The sources of depth data are numerous and have different characteristics. LiDAR systems that are typically used for self-driving scenarios output precise yet sparse depth measurements. This data requires careful filtering and manual processing [8]. Cheap and miniature commodity-grade depth sensors based on active stereo with structured light (*e.g.* Microsoft Kinect), or Time-of-Flight (*e.g.* Microsoft Kinect Azure or depth sensors in many smartphones), provide relatively dense estimates, yet being less accurate and having limited distance range. These sensors are mainly used for indoor scenarios. In several RGB-D datasets such as RedWeb [35] and DIML outdoor [12], stereo pairs serve as a source of depth information. However, the standard procedure based on optical flow does not always provide accurate depth maps, especially for distant objects.

Recently, Structure from Motion (SfM) method has been applied to estimate depth maps via scene reconstruction, *e.g.*, Li *et al.* published the MegaDepth [16] RGB-D dataset that was created using SfM with iterative refinement. The same approach was used in [14] for the Dataset of Frozen People. However, SfM works under assumption that the scene is rigid and does not contain moving objects. Thereby, SfM is mainly applied to reconstruct pieces of architecture or skylines.

While in some of the datasets absolute depth is provided (usually measured by sensors or estimated from aligned stereo cameras with known intrinsics and extrinsics), the others can only offer UTS depth (usually reconstructed by

\*These authors contributed equally to this work

SfM or estimated from aligned stereo cameras with unknown parameters). There are also several datasets containing UTSS inverse depth (from unaligned stereo cameras with unknown parameters).

Overall, none of the existing datasets used separately is sufficient in terms of accuracy, diversity and image quantity for training a robust depth estimation model. This drawback induced various strategies of mixing data from different sources during training [22, 6].

To train models that estimate depth in absolute values, only absolute depth can be used. UTS models can be trained on both absolute and UTS data. Recently, Ranftl *et al.* [22] proposed to train a UTSS model on absolute, UTS and UTSS data from different sources. The resulting model demonstrated an impressive generalization ability. However, UTSS models have a serious drawback of not being able to reconstruct scene geometry. Therefore, we aim to train a UTS model using the same depth data of different types.

Following [22], we train our model on a mixture of datasets. We use the protocol of zero-shot cross-dataset transfer which means that we evaluate our method on completely new datasets unseen on training stage. Through evaluation across several datasets, we prove our method to outperform previous state-of-the-art UTS models.

Our contribution is twofold.

First, we demonstrate that a scale-invariant depth estimation model trained on a mixture of UTS and UTSS data achieves the same accuracy as if it was trained on UTS data only. This opens up possibilities of using large and diverse UTSS datasets to train a method that is able to reconstruct geometry of various unseen environments.

Second, we train several light-weight general-purpose UTS models following the proposed training scheme. Through evaluation, we prove our ideas to be applicable for computationally efficient methods. Thus, our training scheme can be exploited for building applications that make use of depth estimation.

## 2 Related Work

### 2.1 Single-View Depth Estimation

Early methods of general purpose depth estimation from a single RGB image applied complicated heuristic algorithms on hand-crafted features [25, 10]. These methods worked under certain assumptions about the input data that severely narrowed their usage.

Recently, deep learning-based approaches were adopted for solving various computer vision tasks including depth estimation. The majority of modern approaches formulate depth estimation as a dense labelling in continuous space. However, alternative formulations have also been considered: for instance, Fu *et al.* [7] proposed to discretize depth and to interpret depth estimation as ordinal regression problem. In this work, we follow the traditional interpretation.

### 2.2 Encoder-Decoder Architectures

Since we address depth estimation as a dense regression problem, we assume that techniques that appear to be effective for dense labelling tasks might also be applicable for depth estimation. Encoder-decoder architectures with skip connections originally developed for semantic segmentation [23] proved to be capable of solving a wide range of tasks. This approach allows to combine a pre-trained backbone serving as feature extractor with various decoder architectures.

A typical feature extractor is a powerful classification network such as ResNet [9] or ResNeXt [36] pre-trained on the large and diverse ImageNet [4] dataset. The strong generalization ability of these models allows to use them for various visual recognition tasks.

### 2.3 Light-Weight Encoder-Decoder Architectures

Unfortunately, the most well-known architectures are too computationally expensive to run in real-time on embedded platforms. In case of limited resources, such light-weight models as MobileNetV2 [11, 24] or EfficientNet [30]) can be used as feature extractors.

A number of efficient decoders, *e.g.* Light-Weight Refine Net [21], EfficientDet [31], and HRNet [33, 28, 29] were originally designed for semantic segmentation and object detection. In Light-Weight Refine Net, deep feature maps are iteratively fused with shallower feature maps. EfficientDet [31] follows similar approach but adds reverse fusion procedure. HRNet implements a slightly different strategy: by processing inputs in several parallel branches with different resolutions, it extracts high-level features and propagates low-level features. As the result, the outputs contain both structural and semantic information so inputs are utilized effectively.

### 2.4 Light-Weight Depth Estimation

While the same light-weight encoders are often used in different efficient architectures solving various problems, the design of decoders tends to be more task-specific.

With computational effectiveness being at the forefront, a proper choice of decoder architecture is crucial. Nekrasov *et al.* [20] performed a search across various neural architectures aiming to find the most compact yet effective decoder block for depth estimation. Alhasim *et al.* [1] made an attempt of balancing performance and accuracy by training a light-weight architecture via transfer learning. Both of aforementioned methods rely on initially efficient decoder architecture. However, there is an alternative approach, *e.g.* in [5, 34], an already trained depth estimation model is then turned light-weight through pruning and quantization.

## 2.5 Absolute, UTS and UTSS Depth Estimation

### 2.5.1 Absolute Depth Estimation.

There are several approaches to address depth estimation problem. The most works are dedicated to estimating absolute depth measured in metric units. However, it is not always possible to determine scale of a scene based on a single image. To acquire absolute depth data, either depth sensor should be used or stereo pairs with corresponding camera extrinsics should be provided. With such requirements, it is difficult to collect the large and diverse dataset for training a depth estimation model.

### 2.5.2 UTS Depth Estimation.

Other approaches focus on estimating depth up to an unknown coefficient. They aim to reconstruct scene geometry rather than predicting distances to the single points of the scene [16]. The UTS data for training such models is easier to acquire, yet the pre-processing requires time and computational resources.

### 2.5.3 UTSS Depth Estimation.

Recently, SVDE method that estimates UTSS depth [22] has been proposed. This approach has a serious drawback: the scene geometry cannot be restored properly if inverse depth shift is unknown. The major strength of this method is the simplicity of data acquisition, as UTSS depth is accessible and easy to process.

In this work, we show that it is possible to train a UTS model using absolute, UTS and UTSS data.

## 3 Proposed Method

### 3.1 Architectures

In this work, we aim for developing a practical solution and try to find a proper balance between accuracy and computational efficiency.

Following the approach by Ranftl *et al.* [22], we use a RefineNet approach to address depth estimation problem but make it light-weight.

#### 3.1.1 Encoders.

The encoders are based either on MobileNetv2 [24] or architectures from EfficientNet [30] family (namely EfficientNet-Lite0, EfficientNet-b0, b1, b2, b3, b4, b5) pre-trained on ImageNet classification task.

#### 3.1.2 Decoder.

Our decoder architecture is based on vanilla Light-Weight Refine Net decoder[21]. We introduce two modifications to satisfy efficiency requirements and to address stability issues. First, we replace the layer that maps encoder output to 256 channels. We use Fusion Block that does not change the number of channels instead. In this block, the output of the encoder layer is fused with the features coming from a deeper layer (see Figure 1, left). Second, we noticed that original Chained Residual Pooling (CRP) blocks prevents the model from converging. We fix this issue by replacing summation with averaging (see Figure 1, right). Hereinafter, we will refer to this decoder architecture as to **LRN**.

The described networks output predictions that are twice as small as target depth maps, so we upscale them to the original resolution via bilinear interpolation. These outputs are interpreted as depth values in logarithmic scale.

### 3.2 Loss Function

#### 3.2.1 Scale Invariant Loss.

In this work, we propose an *L1* pairwise loss function which can be calculated as follows:

$$\mathcal{L}_{SI} = \frac{1}{N^2} \sum_{i,j=0}^N |(d_i - d_j) - (d_i^* - d_j^*)|, \quad (1)$$

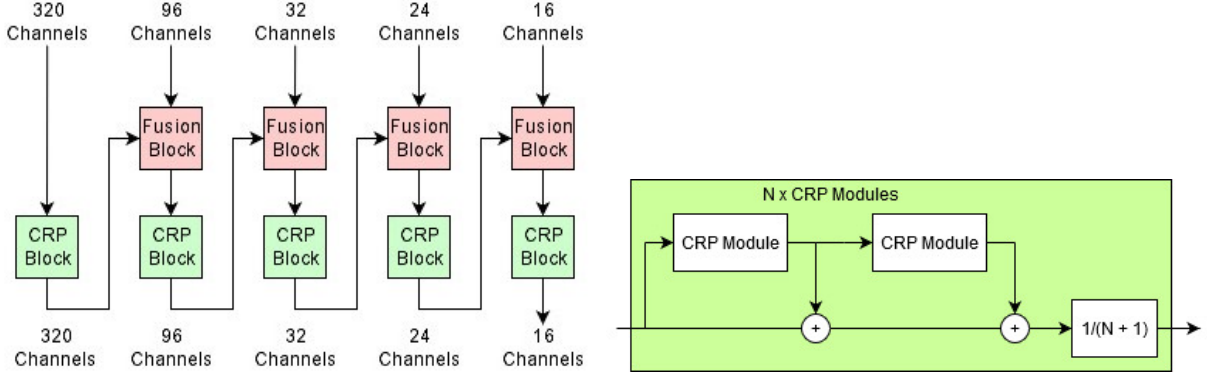


Figure 1: **Left:** LRN branch. Number of fusion block output channels is equal to number of channels on the corresponding level. **Right:** CRP block fix. If CRP block has  $N$  CRP modules, the output signal should be divided by  $N + 1$ .

where  $d$  is a predicted logarithm of depth and  $d^*$  is a logarithm of a ground truth depth.

The proposed  $L1$  pairwise loss is scale-invariant (SI) so it can be used for training on both absolute and UTS depth maps.

To calculate this loss, the summation is performed across  $N^2$  terms. However, it can be computed more efficiently in  $O(N \log N)$  time. Let  $R_{\{i\}}$  denote the list of differences between ground truth and predicted depth values ranged in increasing order:  $R_i = d_i - d_i^*$ . After rearranging and grouping similar terms, the  $L1$  pairwise loss formula can be written as:

$$\mathcal{L}_{SI} = -\frac{2}{N^2} \sum_{i=1}^N R_{\{i\}} (N - 1 - 2(i - 1)), \quad (2)$$

where  $R_{\{i\}}$  is a sorted set of  $R_i$ :  $R_{\{i\}} \geq R_{\{j\}}$  if  $i > j$ . To sort the list of differences, we need  $O(N \log N)$  operations,  $\mathcal{L}_{SI}$  is computed in linear time. Overall, the computational cost of calculating  $L1_{SI}$  pairwise loss is  $O(N \log N)$ .

### 3.2.2 Shift-and-Scale Invariant Loss.

SI loss may be easily converted to shift-and-scale invariant (SSI) loss. Following [22], we replace a logarithm of depth  $d$  with a normalized depth:

$$\tilde{D}_i = \frac{D_i - \mu}{\sigma}, \quad (3)$$

where  $\mu$  and  $\sigma$  are mean and standard deviation of a single depth map. Having this in mind, we can define the SSI  $L1$  pairwise loss:

$$\mathcal{L}_{SSI} = \frac{1}{N^2} \sum_{i,j=0}^N |(\tilde{D}_i - \tilde{D}_j) - (\tilde{D}_i^* - \tilde{D}_j^*)|. \quad (4)$$

Thus, having a mixture of UTS and UTSS ground truth, we can use SI loss for training on UTS data and SSI loss for training on both UTS and UTSS data.

## 4 Experiments

### 4.1 Experimental Setup

#### 4.1.1 Augmentations.

In all the experiments, we use the same set of augmentations implemented in albumentations library.

Specifically, we apply resizing, padding and taking random crops to obtain images and depth maps of size  $384 \times 512$ . We use geometrical transforms such as rotating and flipping images and also apply color manipulations.

#### 4.1.2 Optimization.

The model parameters are optimized via Ranger algorithm which is a modification of Adam optimizer [13] equipped with LookAhead [38] and Radam [17]. Learning rate is set to  $10^{-3}$ , each minibatch contains 32 samples for MobileNet v2, EfficientNet-lite0, b0, b1, b2, 16 samples for EfficientNets b3, b4, b5.

### 4.1.3 Implementation Details.

We implement all models in Python 3.6 using Setka<sup>1</sup> framework based on PyTorch. We use EfficientNets from Segmentation Models Pytorch [37]. The experiments are performed with NVidia Tesla P40 GPU.

## 4.2 Metrics

To evaluate our method, we use standard metrics for depth estimation. Namely, we calculate  $\delta1.25$ ,  $\delta1.25^2$ ,  $\delta1.25^3$ ,  $\log_{10}$  and rel. Since we estimate depth up to scale, we need to align predictions and ground truth in scale prior to calculating metrics. We select the depth scale that minimizes the  $\log_{10}$  metric on validation subset (i.e., we add a median of  $d^* - d$  over the image).

## 4.3 Datasets

Across all the experiments, we use the same set of datasets for training and testing unless otherwise stated. Namely, we train our models on a mixture of RedWeb [35], DIML [12], 3D Movies [22], and MegaDepth [16] datasets and evaluate them on previously unseen NYUv2 Raw [19], TUM-RGBD [26], DIW [3], and KITTI [8] datasets. In the brief description below, we highlight the key features of the datasets.

Dataset	Scene type	Scene motion	Dense/ sparse	Depth source	Depth type	Image size	#Samples
DIML Indoor [12]	indoor	static	dense	sensor	absolute		220K
MegaDepth [16]	general	dynamic	dense	SfM	UTS		130K
ReDWeb [35]	general	dynamic	dense	stereo	UTSS		3600
3D Movies [22]	general	dynamic	dense	stereo	UTSS	1880×800	75K
Sintel [2]	general	dynamic	dense	synthetic	absolute		1064
NYUv2 Raw [19]	indoor	dynamic	dense	sensor	absolute	640×480	407K
TUM-RGBD [26]	indoor	dynamic	dense	sensor	absolute	640×480	80K
DIW [3]	general	dynamic	sparse	user clicks	ordinal		496K
KITTI [8, 18]	outdoor	dynamic	dense	stereo	absolute	1224×368	93K

Table 1: Overview of the datasets used in our experiments

### 4.3.1 RedWeb [35].

The ReDWeb dataset consists of 3600 stereo RGB-D images covering both indoor and outdoor scenarios. This is a small yet carefully curated and highly diverse dataset with dynamic scenes.

### 4.3.2 DIML [12].

The large-scale DIML dataset covers more than 200 indoor and outdoor environments. Following [22], we use only indoor data in the form of synchronized RGB-D frames from both Kinect v2 and stereo camera.

### 4.3.3 3D Movies [22].

The 3D Movies dataset was proposed by the authors of MiDaS [22]. It consists of 23 movies and features video frames from various non-static environments. We reproduced the original data acquisition approach yet we used RAFT [32] instead of PWCNet [27] to estimate disparity. We have also used additional set of 14 stereomovies.

### 4.3.4 MegaDepth [16].

The MegaDepth dataset covers 196 predominantly static indoor and outdoor scenes most of which are architectural landmarks.

### 4.3.5 NYUv2 Raw [19].

NYUv2 Raw is a common benchmark for depth estimation. It contains more than 300K RGB images accompanied by raw depth maps acquired via Kinect sensor.

<sup>1</sup><https://github.com/RomanovMikeV/setka>

#### 4.3.6 TUM-RGBD [26].

The TUM-RGBD dataset is a benchmark for visual odometry and visual SLAM systems. It contains the color images and depth measurements from Kinect sensor that were captured asynchronously and thus have to be matched and spatially aligned. For our experiments, we select only non-static scenes that feature humans in indoor environments [15].

#### 4.3.7 KITTI [8, 18].

The KITTI dataset is the standard benchmark used for the various computer vision tasks, like optical flow estimation [8, 18], visual odometry [8], depth estimation [8, 18], object detection [8], etc. It contains outdoor scenes from "city", "residential" and "road" categories.

#### 4.3.8 Sintel [2].

Sintel is the only synthetic dataset in the mixture. Accordingly, it features perfect ground truth depth maps for dynamic synthetic scenes.

#### 4.3.9 DIW [3].

The DIW dataset is a large-scale and highly diverse dataset containing both indoor and outdoor scenes crawled from Flickr. Depth data was acquired via manual labelling in a form of sparse ordinal relations.

### 4.4 Results

#### 4.4.1 Proof of Concept on NYUv2 Raw.

As a proof-of-concept, we train a UTS model on a mixture of UTS and UTSS data from the NYUv2 Raw dataset.

Since NYUv2 Raw contains absolute depth, we can make it either UTS or UTSS. To convert absolute depth to UTS, we multiply it by a random positive coefficient. To obtain UTSS data, we multiply the inverse depth by a random scale and then shift it by a random value.

To obtain comprehensive results, we create a few mixtures where UTS and UTSS data is present in different proportions. For a given  $p$ ,  $p\%$  of the source absolute data is converted to UTS data and the rest is converted to UTSS data.

For the proof-of-concept, we use a light-weight model that consists of MobileNet encoder and LRN decoder. We train this model on each UTS / UTSS mixture using the following loss function:

$$\mathcal{L}_{Mixture} = I_{UTS} \mathcal{L}_{SI} + \mathcal{L}_{SSI}, \quad (5)$$

where  $I_{UTS}$  is 1 for the UTS data and 0 for UTSS data. We evaluate this model against the same model that was trained only on the UTS data.

The results of this experiments are depicted in the Fig. 2. The model trained on the UTS data demonstrates expected behaviour: the more training data we use, the better results we obtain. At the same time, the model trained on the mixture of UTS and UTSS data shows similar results for all  $p$ . In other words, it performs as if it was trained on the dataset fully supplied with UTS data.

We propose an explanation of the observed phenomenon.

With the improper shift, the straight lines on the image turn into the curves in the frustum and the pairwise distances between scene points are not preserved. Therefore, it is necessary to know shift value in order to reconstruct the geometry of the scene.

During training on UTSS data, the network attempts to estimate shift and relative depth jointly which resembles multi-task learning. We assume that it helps to restore scene geometry more precisely.

The proof-of-concept demonstrates that a UTS model can be successfully trained on a mixture of UTS and UTSS data.

#### 4.4.2 Full-featured Training on UTS and UTSS Data.

Among training datasets, only MegaDepth and DIML contain UTS data. Consequently, we can train on these two datasets in UTS mode and on MegaDepth, DIML, 3D Movies, and RedWeb in UTSS mode. As shown in Table 2, by using our training scheme we manage to significantly improve the results.

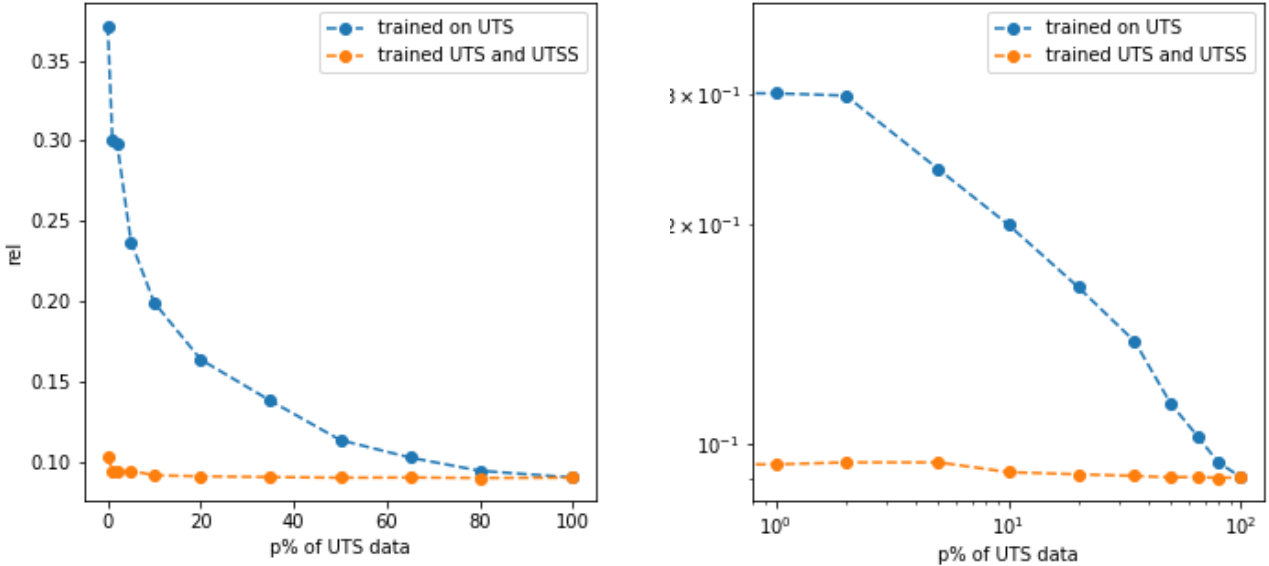


Figure 2: Results of the models trained on the UTS data and on the mixture of the UTS and UTSS data. *Left*: rel against percentage  $p$  of the UTS data in the mixture. *Right*: Same, in logarithmic scale.

Method	Data	NYUv2	TUM	KITTI	Sintel	DIW
MN-LRN	UTS	14.95	16.56	39.17	0.435	20.96
EfficientNet-Lite0-LRN	UTS	13.69	16.54	35.85	0.438	19.57
MN-LRN	UTS+UTSS	14.03	14.43	37.95	0.365	15.04
EfficientNet-Lite0-LRN	UTS+UTSS	13.70	13.24	32.85	0.353	14.30

Table 2: Results of the models trained on UTS and combined UTS and UTSS data.

#### 4.4.3 Light-Weight Models.

Besides, we measure generalization ability of light-weight models.

We demonstrate the results of our light-weight models in Tab. 3. The proposed method demonstrates a good generalization to the unseen datasets. The qualitative results may be found on figure 3. The visualized meshes may be found on the figure 4.

Method	NYU	TUM	KITTI	Sintel	DIW	Params	MAdds	FPS
MiDaS* [22]	9.55	14.29	23.9	0.327	12.46	105.4	103.9	37
Li et al. [16]	34.39	33.11	47.68	0.490	24.55	5.4	91.1	63
Mannequin [14]	23.42	22.39	40.86	0.431	26.52	5.4	91.1	63
MN-LRN	14.03	14.43	37.95	0.365	15.04	2.4	1.17	135
EfficientNet-Lite0-LRN	13.70	13.24	32.85	0.353	14.30	3.6	1.29	127
EfficientNet-B0-LRN	13.28	15.18	28.77	0.334	13.15	4.2	1.66	82
EfficientNet-B1-LRN	12.04	15.66	27.45	0.312	12.79	6.7	2.22	63
EfficientNet-B2-LRN	12.39	15.87	25.11	0.321	12.92	8	2.5	62
EfficientNet-B3-LRN	11.47	14.09	23.40	0.336	12.95	11	3.61	57
EfficientNet-B4-LRN	11.07	13.49	22.62	0.325	12.96	18	5.44	47
EfficientNet-B5-LRN	10.85	12.84	23.16	0.308	13.15	29	8.07	40

Table 3: Results of the UTS models trained on the datasets mixtures of UTS and UTSS data compared to other single-view depth estimation methods. For each model, number of parameters (Params), number of multiply-addition operations (MAdds) and frame rate (FPS) are estimated for  $384 \times 384$  inputs. Training of the algorithms is performed on  $384 \times 384$  crops, while the inference is performed on the images with shortest side rescaled to 384 pixels with fixed side ratio. \*The performance of MiDaS [22] is measured using UTSS metrics, for the other models UTS metrics are used.

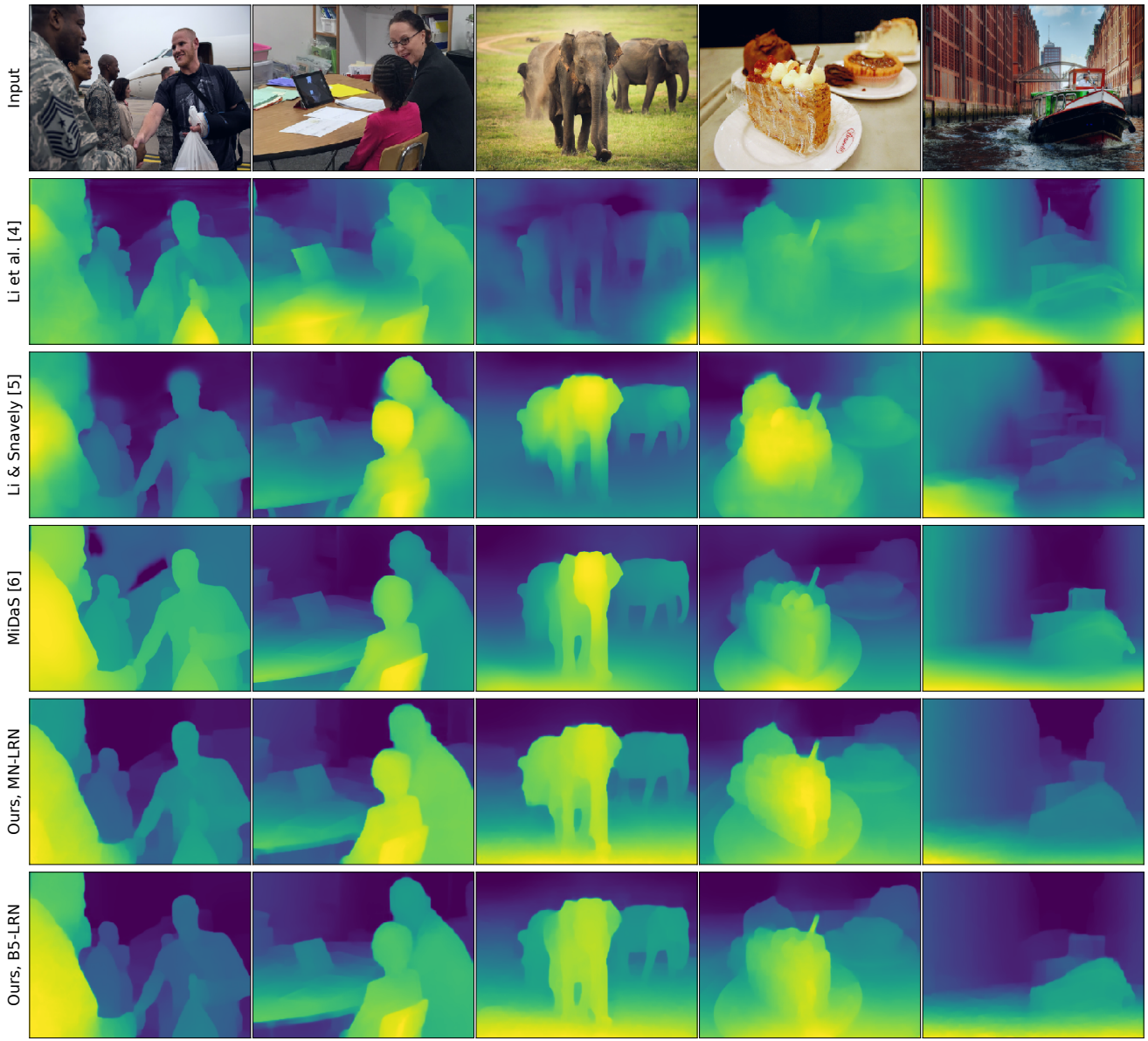


Figure 3: Qualitative comparison of our light-weight models trained on datasets mixture. Images are mainly taken from DIW dataset and were not seen during training. We also include results of MiDaS [22] method as a reference.

## 4.5 Discussion

### 4.5.1 Training on UTS and UTSS Data.

The acquisition of the UTS data is often a bottleneck. At the same time, the sources of UTSS stereo data are accessible, diverse and aplenty.

Through evaluation, we prove that we can train a UTS model on UTSS data. Hence, the requirements for the training data can be significantly reduced. This broadens horizons for production-ready solutions. We argue that stereo data gathered from multiple sources provides a solid basis for a versatile and robust single-view depth estimation method.

### 4.5.2 Limitations of Stereo Matching.

Obtaining depth maps via stereo matching has certain limitations. First, precise disparities for distant objects can be obtained from a very wide stereo baseline. Besides, the method depends massively on the model used to estimate the disparity. To estimate depth in the distance, it should be sensitive enough to capture small displacements. Accordingly, single-view depth estimation is not yet applicable for large-scale scenarios such as outdoor landscapes.

#### 4.5.3 Limitations of Light-weight Models.

Furthermore, the light-weight models are not capable of producing the sharp depth maps yet. Still, there is a trade-off between the accuracy of depth estimates and the complexity of the model which determines speed of the inference, memory requirements and power consumption.

## 5 Conclusion

In this paper, we aimed for building a light-weight general-purpose monocular single-view UTS depth estimation model. We have shown that it is possible to train a scale-invariant depth estimation model on a mixture of UTS and UTSS data. This training scheme allows us to simultaneously use large and diverse UTSS data and reconstruct the scene geometry by using a small amount of UTS data. In some cases, the resulting model is as accurate as if it was trained on UTS data of the same volume.

Then, we trained several EfficientNet-based networks to demonstrate the capabilities of our approach. The experimental evaluation proved that our ideas are applicable to light-weight models. We assume that our training scheme might be helpful for applications that perform depth estimation in various scenarios and with limited resources.

## References

- [1] I. Alhashim and P. Wonka. High quality monocular depth estimation via transfer learning, 2018.
- [2] D. Butler, J. Wulff, G. Stanley, and M. Black. A naturalistic open source movie for optical flow evaluation. pages 611–625, 10 2012.
- [3] W. Chen, Z. Fu, D. Yang, and J. Deng. Single-image depth perception in the wild. In D. D. Lee, M. Sugiyama, U. V. Luxburg, I. Guyon, and R. Garnett, editors, *Advances in Neural Information Processing Systems 29*, pages 730–738. Curran Associates, Inc., 2016.
- [4] J. Deng, W. Dong, R. Socher, L.-J. Li, K. Li, and L. Fei-Fei. Imagenet: A large-scale hierarchical image database. In *2009 IEEE conference on computer vision and pattern recognition*, pages 248–255. Ieee, 2009.
- [5] S. Elkerdawy, H. Zhang, and N. Ray. Lightweight monocular depth estimation model by joint end-to-end filter pruning. *2019 IEEE International Conference on Image Processing (ICIP)*, Sep 2019.
- [6] J. M. Facil, B. Ummenhofer, H. Zhou, L. Montesano, T. Brox, and J. Civera. Cam-conv: Camera-aware multi-scale convolutions for single-view depth, 2019.
- [7] H. Fu, M. Gong, C. Wang, K. Batmanghelich, and D. Tao. Deep ordinal regression network for monocular depth estimation, 2018.
- [8] A. Geiger, P. Lenz, and R. Urtasun. Are we ready for autonomous driving? the kitti vision benchmark suite. In *Conference on Computer Vision and Pattern Recognition (CVPR)*, 2012.
- [9] K. He, X. Zhang, S. Ren, and J. Sun. Deep residual learning for image recognition, 2015.
- [10] D. Hoiem, A. Efros, and M. Hebert. Geometric context from a single image. volume 1, pages 654– 661 Vol. 1, 11 2005.
- [11] A. G. Howard, M. Zhu, B. Chen, D. Kalenichenko, W. Wang, T. Weyand, M. Andreetto, and H. Adam. Mobilenets: Efficient convolutional neural networks for mobile vision applications, 2017.
- [12] Y. Kim, H. Jung, D. Min, and K. Sohn. Deep monocular depth estimation via integration of global and local predictions. *IEEE Transactions on Image Processing*, PP:1–1, 05 2018.
- [13] D. P. Kingma and J. Ba. Adam: A method for stochastic optimization, 2014.
- [14] Z. Li, T. Dekel, F. Cole, R. Tucker, N. Snavely, C. Liu, and W. T. Freeman. Learning the depths of moving people by watching frozen people. *CoRR*, abs/1904.11111, 2019.
- [15] Z. Li, T. Dekel, F. Cole, R. Tucker, N. Snavely, C. Liu, and W. T. Freeman. Learning the depths of moving people by watching frozen people, 2019.
- [16] Z. Li and N. Snavely. Megadepth: Learning single-view depth prediction from internet photos. In *Computer Vision and Pattern Recognition (CVPR)*, 2018.

[17] L. Liu, H. Jiang, P. He, W. Chen, X. Liu, J. Gao, and J. Han. On the variance of the adaptive learning rate and beyond, 2019.

[18] M. Menze and A. Geiger. Object scene flow for autonomous vehicles. In *Conference on Computer Vision and Pattern Recognition (CVPR)*, 2015.

[19] P. K. Nathan Silberman, Derek Hoiem and R. Fergus. Indoor segmentation and support inference from rgbd images. In *ECCV*, 2012.

[20] V. Nekrasov, H. Chen, C. Shen, and I. Reid. Fast neural architecture search of compact semantic segmentation models via auxiliary cells, 2018.

[21] V. Nekrasov, C. Shen, and I. Reid. Light-weight refinenet for real-time semantic segmentation, 2018.

[22] R. Ranftl, K. Lasinger, D. Hafner, K. Schindler, and V. Koltun. Towards robust monocular depth estimation: Mixing datasets for zero-shot cross-dataset transfer, 2019.

[23] O. Ronneberger, P. Fischer, and T. Brox. U-net: Convolutional networks for biomedical image segmentation, 2015.

[24] M. Sandler, A. Howard, M. Zhu, A. Zhmoginov, and L.-C. Chen. Mobilenetv2: Inverted residuals and linear bottlenecks, 2018.

[25] A. Saxena, M. Sun, and A. Y. Ng. Make3d: Learning 3d scene structure from a single still image. *IEEE Transactions on Pattern Analysis and Machine Intelligence*, 31(5):824–840, 2009.

[26] J. Sturm, N. Engelhard, F. Endres, W. Burgard, and D. Cremers. A benchmark for the evaluation of rgbd slam systems. In *Proc. of the International Conference on Intelligent Robot Systems (IROS)*, Oct. 2012.

[27] D. Sun, X. Yang, M.-Y. Liu, and J. Kautz. Pwc-net: Cnns for optical flow using pyramid, warping, and cost volume. In *Proceedings of the IEEE conference on computer vision and pattern recognition*, pages 8934–8943, 2018.

[28] K. Sun, B. Xiao, D. Liu, and J. Wang. Deep high-resolution representation learning for human pose estimation. In *CVPR*, 2019.

[29] K. Sun, Y. Zhao, B. Jiang, T. Cheng, B. Xiao, D. Liu, Y. Mu, X. Wang, W. Liu, and J. Wang. High-resolution representations for labeling pixels and regions. *CoRR*, abs/1904.04514, 2019.

[30] M. Tan and Q. V. Le. Efficientnet: Rethinking model scaling for convolutional neural networks, 2019.

[31] M. Tan, R. Pang, and Q. V. Le. Efficientdet: Scalable and efficient object detection, 2019.

[32] Z. Teed and J. Deng. Raft: Recurrent all-pairs field transforms for optical flow. *arXiv preprint arXiv:2003.12039*, 2020.

[33] J. Wang, K. Sun, T. Cheng, B. Jiang, C. Deng, Y. Zhao, D. Liu, Y. Mu, M. Tan, X. Wang, W. Liu, and B. Xiao. Deep high-resolution representation learning for visual recognition, 2019.

[34] Wofk, Diana and Ma, Fangchang and Yang, Tien-Ju and Karaman, Sertac and Sze, Vivienne. FastDepth: Fast Monocular Depth Estimation on Embedded Systems. In *IEEE International Conference on Robotics and Automation (ICRA)*, 2019.

[35] K. Xian, C. Shen, Z. Cao, H. Lu, Y. Xiao, R. Li, and Z. Luo. Monocular relative depth perception with web stereo data supervision. In *The IEEE Conference on Computer Vision and Pattern Recognition (CVPR)*, June 2018.

[36] S. Xie, R. Girshick, P. Dollár, Z. Tu, and K. He. Aggregated residual transformations for deep neural networks, 2016.

[37] P. Yakubovskiy. Segmentation models pytorch. [https://github.com/qubvel/segmentation\\_models.pytorch](https://github.com/qubvel/segmentation_models.pytorch), 2020.

[38] M. R. Zhang, J. Lucas, G. Hinton, and J. Ba. Lookahead optimizer: k steps forward, 1 step back, 2019.

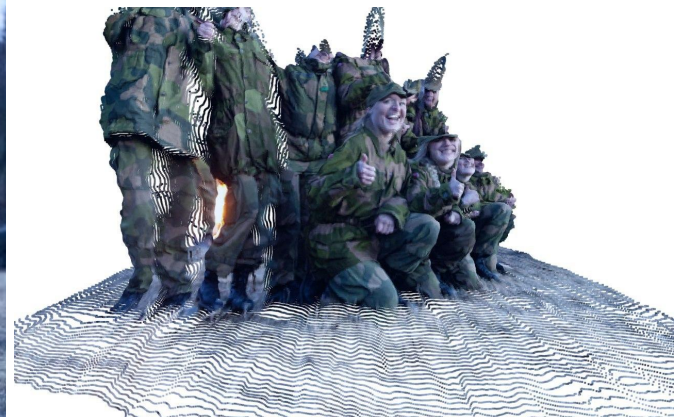


Figure 4: Images and the corresponding 3D mesh reconstructed using depth map predicted by b5-LRN model.